POLITECNICO DI TORINO
Repository ISTITUZIONALE

Experimental Study of Desorption and Seepage Characteristics of Single Gas and CO2–CH4 Gas Mixture in Coal

Original
Experimental Study of Desorption and Seepage Characteristics of Single Gas and CO2–CH4 Gas Mixture in Coal / Yu, B., Zhang, D., Xu, B., Xiao, W., Wang, C., Du, W.. - In: NATURAL RESOURCES RESEARCH. - ISSN 1520-7439. - 31:5(2022), pp. 2715-2730. [10.1007/s11053-022-10077-0]

Availability:
This version is available at: 11583/2997261 since: 2025-02-06T14:28:40Z

Publisher:
Springer

Published
DOI:10.1007/s11053-022-10077-0

Terms of use:

This article is made available under terms and conditions as specified in the corresponding bibliographic description in the repository

Publisher copyright
Springer postprint/Author's Accepted Manuscript

This version of the article has been accepted for publication, after peer review (when applicable) and is subject to Springer Nature’s AM terms of use, but is not the Version of Record and does not reflect post-acceptance improvements, or any corrections. The Version of Record is available online at: http://dx.doi.org/10.1007/s11053-022-10077-0

(Article begins on next page)

17 November 2026

Experimental study on fatigue life of gypsum-like rock under uniaxial compression with different loading frequencies

Wang Chongyang[1,2], Wei Sijiang[1,3], Pan Yisha[4], Zhang Sheng[5]

1-School of Energy Science and Engineering, Henan Polytechnic University, Jiaozuo 454000, Henan, China.

2-College of Resources and Security, Chongqing University, Chongqing 400044, China.

3- Collaborative Innovation Center of Coal Work Safety and Clean High Efficiency Utilization, Jiaozuo 454000, Henan, China.

4-School of Surveying, Mapping and Land Information Engineering, Henan Polytechnic University, Jiaozuo 454000, Henan, China.

5-Luxshare Precision Industry (Chuzhou), Ltd, Chuzhou 239000, Anhui, China.

* Correspondence: jzitwsj@126.com

Abstract: When the surrounding rock is subjected to cyclic loading, its physical and mechanical properties will show fatigue damage properties under the action of periodic engineering, disturbance stress. In this research, the fatigue life test of gypsum-like rocks was carried out by using a dynamic fatigue testing machine. During the cyclic loading process, the maximum fatigue loading times increased with the increase of frequency, but the fatigue life increased first and then decreased with the increase of frequency. The stress-circumferential strain hysteresis loop of the specimen tilts to ε axis at low frequency and to σ axis at high frequency, which indicates that the lower the frequency is, the greater the damage of the specimen is in one cycle. The strain of the sample increases with time, and the action mechanism of fatigue loading can be divided into three stages: initial stage, stable development stage, and failure stage. It was observed that under the conventional uniaxial compression test conditions, the failure mode of specimens is shear failure. The end effect of specimens after fatigue loading is more obvious, and the failure modes are mainly the fatigue damage of near vertical cracks. After fatigue loading, the specimen has obvious fatigue damage. With the expansion and penetration of the internal crack, the width, length and coverage of the crack gradually increase, leading to the continuous deterioration of the physical and mechanical properties.

Key words: high strength gypsum; fatigue life; acoustic emission; failure characteristics

Declarations

Funding: This work was supported by National Natural Science Foundation of China (No. 51974104).

Conflicts of Interest: The authors declare no conflict of interest.

Availability of data and material: All test data comes from laboratory tests which is accurate and solid.

Code availability: Not applicable.

Author Contributions: Wei Sijiang supervised the research and proposed the research direction. Wang Chongyang was responsible for the laboratory test, report analysis and paper writing. Pan Yisha helped in writing the paper. Zhang Sheng helped with some laboratory test.

Ethics approval: Consent.

Consent to participate: Agree to participate.

Consent for publication: Agreement for publication.

Article Highlights

1) During the cyclic loading process, the maximum fatigue loading times increases with the increase of frequency, but the fatigue life first increases and then decreases with the increase of frequency.

2) During fatigue loading, the lower the frequency, the greater the damage of the specimen in one cycle.

3) After fatigue loading, the specimen has obvious fatigue damage. With the expansion and penetration of the internal crack, the width, length and coverage of the crack gradually increase, the continuous deterioration of the physical and mechanical properties.

1. Introduction

Common underground engineering is often affected by dynamic fatigue load, which has a great influence on the stability of these engineering. In particular, the blasting load and abutment pressure formed by periodic pressure in coal mining environment and dynamic load of underground engineering under earthquake action all have the characteristics of repeated loading and periodicity. These dynamic loads are essential to the long-term stability and life of underground engineering. Therefore, it is of great significance to study the fatigue life of rock under cyclic loading.

Scholars at home and abroad have very rich research results on the fatigue properties of rocks. Many scholars have studied the effect of loading frequency on fatigue characteristics from the perspective of frequency and stress limit (Zhao et al., 2013; Liu et al., 2001; Li et al., 2020; Roohollah Shirani Faradonbeh et al.,2020). Some scholars have found that the fatigue strength of rock increases with the increase of loading frequency and amplitude (Bagde M N et al., 2005; Li n et al., 2001; Ishizuka Y et al., 1990); Other scholars believe that the higher the loading rate is, the faster the crack in the rock will expand and the faster the rock failure rate will be (Jiang et al.,2003; Xiao 2009). Many scholars have also discussed the deformation and energy change of rock during fatigue loading (Zuo et al., 2011; Yang et al., 2007; Bai et al., 2012; Li et al., 2016; Xu et al., 2006; Xi et al.,2003). For example, through fatigue experiments, it is concluded that the axial strain of salt rock during fatigue failure can be divided into three stages: initial deformation, constant deformation and accelerated deformation (Guo et al., 2011). According to the damage, deformation and energy characteristics of rock under different confining pressures, cyclic loading and unloading tests were carried out to obtain the law of energy transformation in the process of rock damage and failure (Zhao et al.,2013). Some scholars have studied the fatigue mechanical properties of jointed rock under different loading conditions (Liu et al.,2012, 2017, 2018a, 2018b; Zhang et al.,2018). They believe that it is beneficial for rational design and stability analysis of rock engineering projects to understanding the fatigue mechanical properties of jointed rocks. And it is concluded that under lower loading frequency or higher maximum stress and amplitude, the jointed specimen is characterized by higher fatigue deformation moduli and higher dissipated hysteresis energy, resulting in higher cumulative damage and lower fatigue life. Some scholars explored the fatigue life characteristics of rock mass through numerical simulation. For example, the finite difference method was used to establish the coupling calculation model between the tunnel and the surrounding rock. Combined with the fatigue life characteristics of the concrete structure at the bottom of the tunnel, the main design parameters of the heavy rail load monorail ballast tunnel lining structure were studied (Ma, W. B et al., 2020).

Although the above scholars have done a lot of research on the fatigue characteristics of rock, there are few reports on the fatigue life characteristics of rock under high stress loading. There are many weak surfaces in coal measure strata and they are large in discretization. However, after being cast for a long time, the artificial cast gypsum rocks have uniform material and small in discretization after being sampled. Moreover, the strength parameters can be adjusted by changing the water content. When exploring mechanical properties, independent variables such as material dispersion can be excluded to the greatest extent to make the results more regular (Wei et al., 2020). On this basis, this kind of rock is selected as the research object and the fatigue life test with loading frequency of 1-20Hz is carried out to explore the influence of loading frequency on the fatigue life of rock. The experimental results can provide reference for the control of surrounding rock in deep foundation pit and underground engineering.

2. Sample characteristics and test methods

2.1 Sample preparation

A grade α high strength gypsum powder, produced by Sichuan Hongtai Biochemical Co., Ltd., Nanchong, China, was selected. Its main component is $CaSO_4 \cdot 0.5H_2O$, and a block was poured according to a ratio of water to

paste of 2.8:10, and a standard sample was processed. The specific preparation process is described in the following:

(1) Mold preparation: A cube mold with a side length of 20 cm was used and lubricating oil was applied on the inner surface to facilitate mold release, as shown in Figure 1(a).

(2) Production of the block: Gypsum powder was evenly poured into water, and the mixture was poured into the mold after full mixing for 90 s with a mixer. The mixture was placed on a vibrating table for 2 min to eliminate bubbles in the slurry and after heat loss, demodulation started. The finished test block is shown in Figure 1(b).

(3) Standard sample processing: After demolding, the test block was shaped into cylindrical standard samples of 50 mm × 100 mm (Φ × h), which were then put into an oven at 45 ℃ for 48 h. At a quality difference between the two adjacent sample of less than 0.5 g, the sample described in this paper were obtained. As shown in Figure 1(c).



(a) (b) (c)

Figure 1. gypsum sample. (a)Casting mould. (b)Cube sample. (c) standard sample

(4) Grouping: The samples were divided into five groups for fatigue life test. The loading methods were shown in Table 1. In the table, σ_{max} is the maximum stress, σ_{min} is the minimum stress, and f is frequency. To improve the reliability of the experimental results, 6 samples were prepared for each group, resulting in a total of 30 samples.

Table 1. Types of fatigue loading test

Group	σ_{max}	σ_{min}	f/Hz
1			1
2			2
3	$0.9\sigma_c$	$0.7\sigma_c$	4
4			10
5			20

It is known from previous tests (Figure 2) that the natural uniaxial strength σ_c of the gypsum-like rock sample used in this paper is about 59.5MPa. The central value ($0.8\sigma_c$) of the fatigue loading conducted within the range of (0.7-0.9) σ_c is located at the damage stress point of the whole stress-strain curve. The loading of (0.7-0.8) σ_c is in the elastic stage, and the loading of (0.8-0.9) σ_c is at the yield stage.

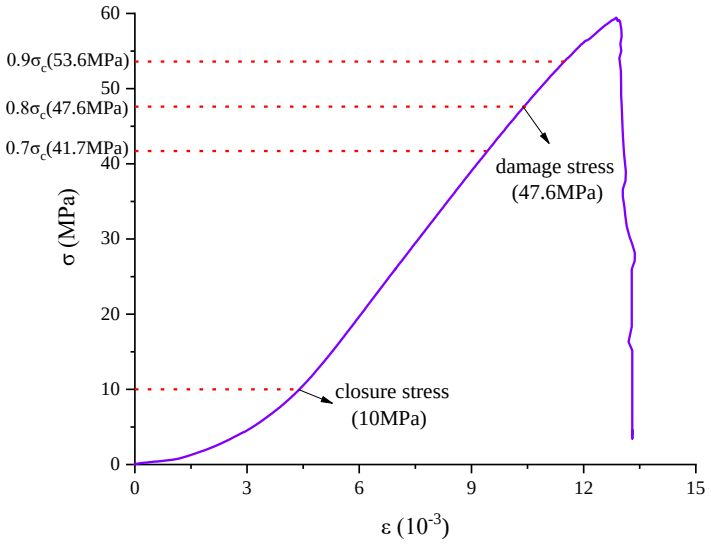


Figure 2. Full stress-strain curve of gypsum rock in natural state

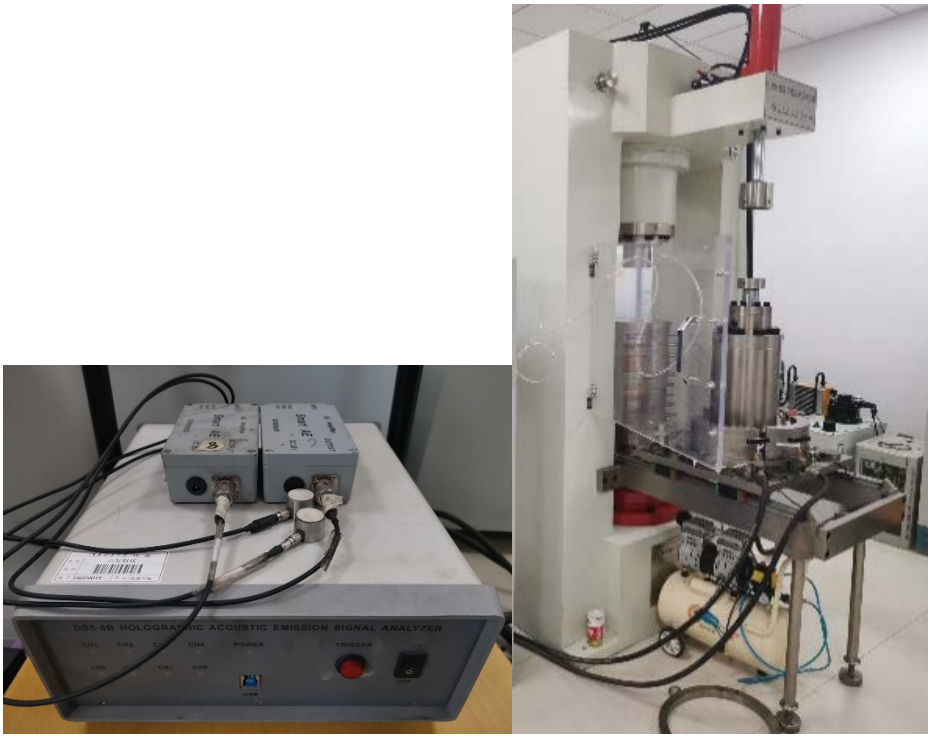
2.2. Testing device

2.2.1. Acoustic emission testing device

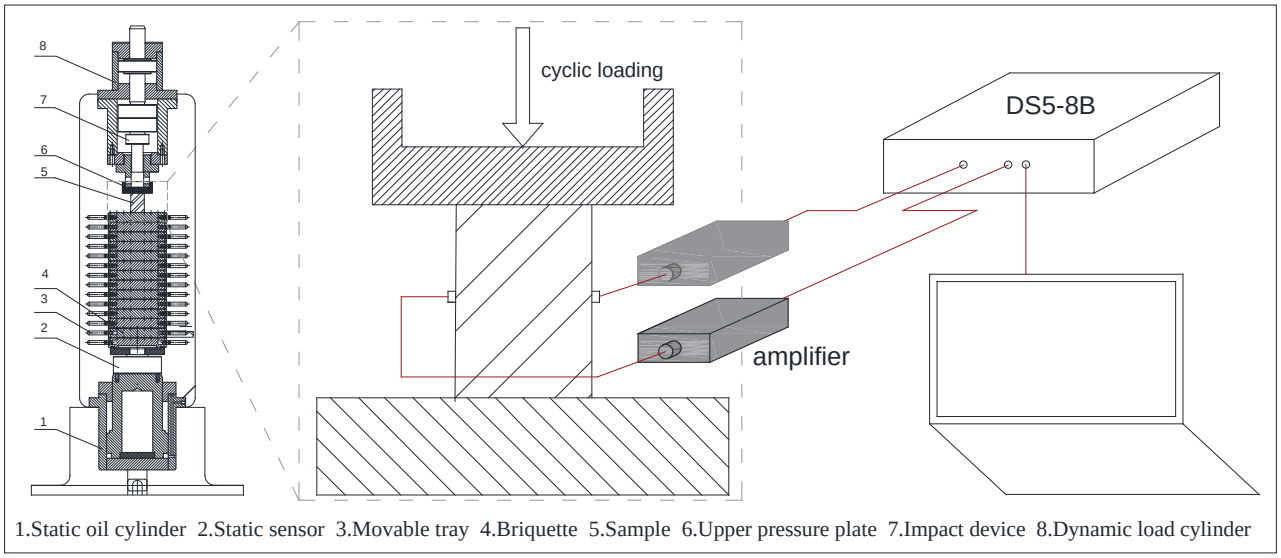
Fracture information (i.e., acoustic emission ringing number and energy) of specimens during fatigue loading and static compression was measured with a DS5-8B holographic acoustic emission signal analyzer, as shown in Figure 3(a). The acoustic emission (AE) instrument adopts a USB3.0 interface with 2-8 channels, and can be used for multi-channel synchronous acquisition. Sampling trigger modes are signal threshold trigger and external trigger. The continuous data pass rate is 65.5 MB/s, and the data pass rate reaches up to 393 MB/s.

2.2.2. Mechanical testing device

A fatigue loading test was carried out on a QKX-YD-1000 electro-hydraulic servo rock dynamic fatigue test machine, which was produced by Qingdao Qiankunxing Intelligent Technology Co., Ltd., Qingdao, Shandong Province. As shown in Figure 3(b) and (c). The maximum axial load of the system is 800 kN, the maximum loading speed is 800 mm/min, the fatigue frequency range is 0.5-50 Hz, and the maximum displacement is 50 mm.



(a) (b)



(c)

Figure 3. Testing device. (a) DS5-8B. (b) QKX-YD-1000 test system. (c) Test principle and wiring diagram.

2.3 Test Methods

(1) Sample size and quality measurement: the vernier caliper is used to measure the sample size and the electronic scale is used to measure the quality.

(2) Fatigue loading test: The axial stress of the sample is loaded to $0.8\sigma_c$ at a loading rate of 0.1mm/min, and then fatigue loading begins. The loading scheme is shown in Table 1. Maximum cycling loads with sinusoidal waveforms will stop automatically after 20000 times. Loading path showed in Figure 4 and v is the loading or unloading rate.

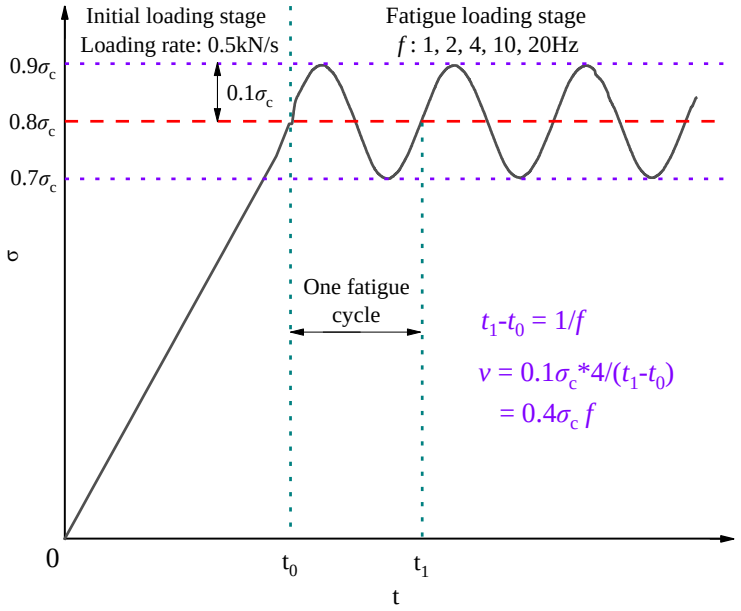


Figure 4. The different stages of loading with their load-control methods.

(3) Acoustic emission characteristics: During the fatigue loading, energy characteristics was monitored with acoustic emission (AE) analyzer. Only two channels were employed because of without spatial positioning.

3.Test Results and Analysis

3.1 Stress-axial strain characteristics

After the fatigue test, all samples in group 1 (f=1Hz) were destroyed, and the average fatigue times was 3 times.

In group 2 (f=2Hz), 4 samples were damaged, and 1 sample was not damaged, and the average fatigue frequency of the damaged specimen was 51 times. In group 3 (f=4Hz), 3 samples were damaged, and 2 samples was not damaged, and the average fatigue frequency of the damaged specimen is 204 times. In group 4 (f=10Hz), 3 samples were damaged, and 2 samples was not damaged, and the average fatigue frequency of the damaged specimen is 400 times. In group 5 (f=20Hz), 1 sample was damaged, and 4 samples were not damaged, and the average fatigue frequency of the damaged specimen is 652 times. The statistical results are shown in Table 2. In the table, n is the number of load cycles when fatigue failure occurs, and T is the time from the beginning of loading to the occurrence of fracture. It is easy to know that:

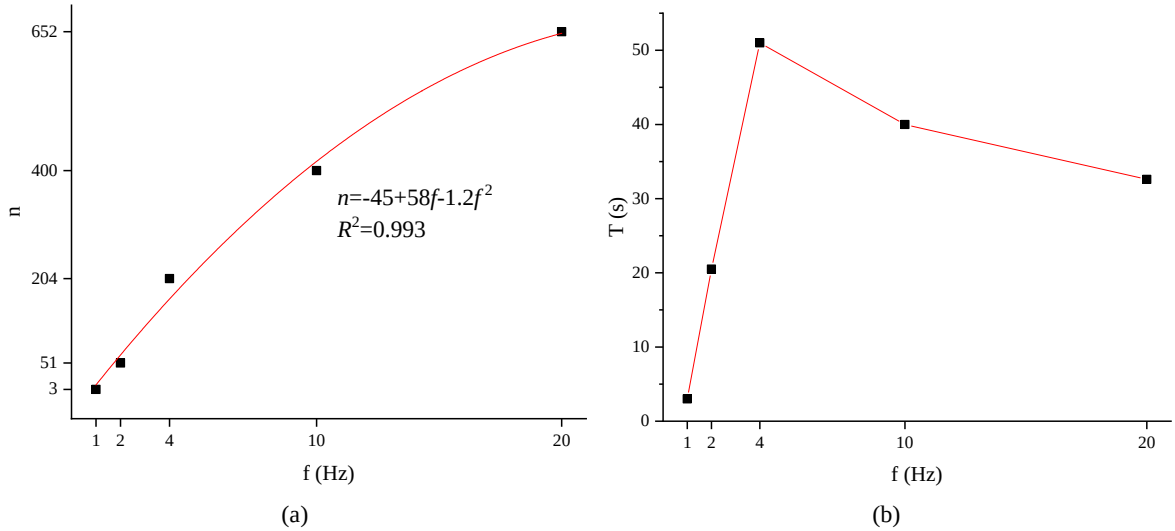
$$T=n/f \qquad (1)$$

Table 2. Fatigue test results

Group	f/Hz	Amount of damage	Damage rate	n	T/s
1	1	5	100%	3	3
2	2	4	80%	51	20.5
3	4	3	60%	204	51
4	10	3	60%	400	40
5	20	1	20%	652	32.6

As can be seen from Table 2, under the condition of constant stress level, the higher the fatigue loading frequency, the lower the proportion of test failure, and the more fatigue times the damaged sample can bear before failure.

To quantitatively analyze the influence of loading frequency f on the fatigue times n and the fatigue life t that can be sustained before failure, the logarithmic function is used to fit the two groups of data, and Figure 5 is obtained.



(a) (b)

Figure 5. Logarithmic fitting of fatigue frequency and frequency. (a)f-n.(b)T-n.

As can be seen from Figure 5(a), the growth rate of fatigue number n decreases with the increase of frequency f, and the two are numerically logarithmic correlated. The relationship is as follows:

$$n=-838+461*\ln(f+5.15) \qquad (2)$$

The confidence of Equation (2) is more than 0.99, The data therefore indicated that the logarithmic fitting function can better reflect the change rule of the two.

At the same time, it can be seen from Figure 5(b) that the fatigue life of the sample increases first and then decreases with the increase of frequency. When $f<4$Hz, the fatigue life t of the sample increases with the increase

of loading frequency. When f=4Hz, the fatigue life T of the sample reaches the peak. When f>4Hz, the fatigue life of the specimen begins to decrease with the increase of loading frequency.

The local diagram of the stress-strain hysteresis loop curve of typical failure sample in each group is shown in Figure 6.

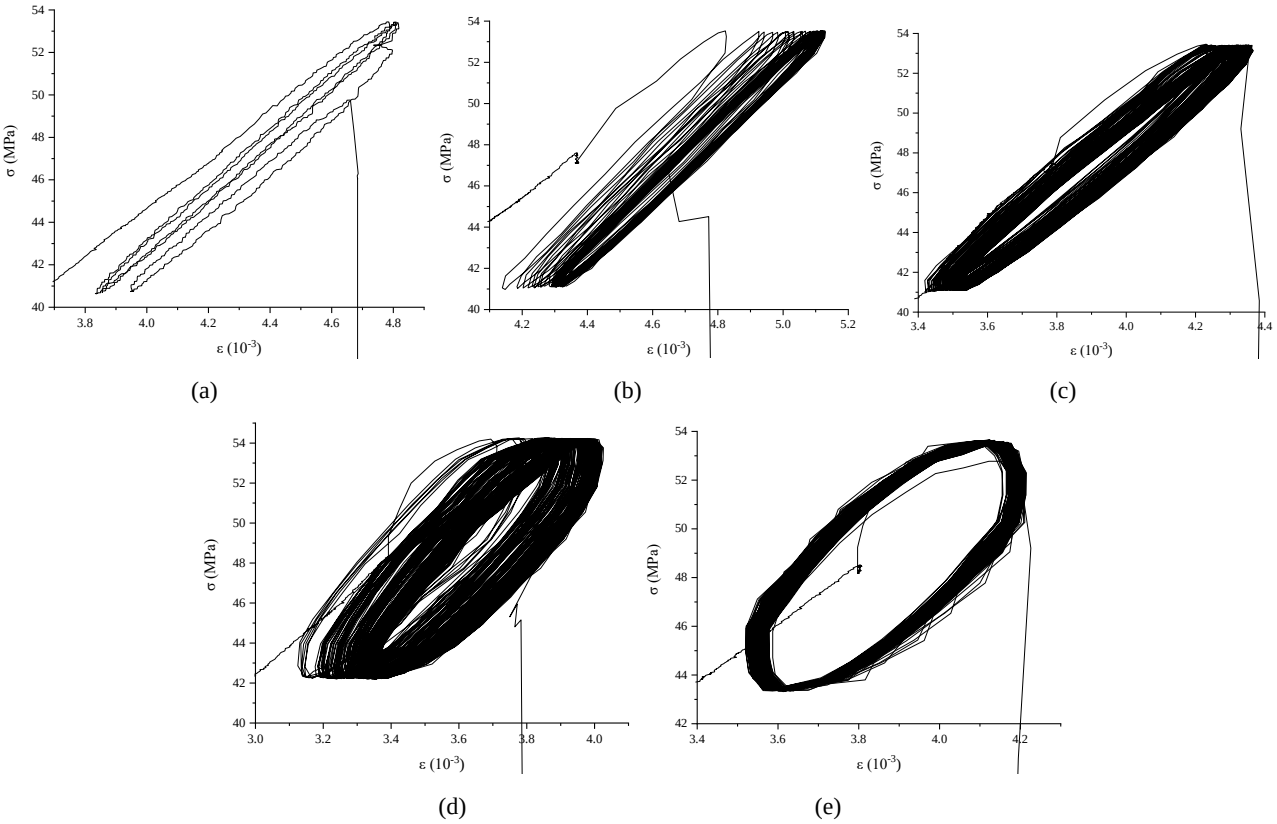


Figure 6. Fatigue loading test curve. (a)f=1Hz. (b)f=2Hz. (c)f=4Hz. (d)f=10Hz. (e)f=20Hz.

As can be seen from Figure 6, the hysteresis loop gradually transitions from a strip to a circle with the increase of fatigue frequency. The higher the frequency, the more obvious the damage. When the loading frequency is low, the load on the sample changes slowly and the stress-strain curve is relatively flat, as shown in Figure 6 (a) and (b). With the increase of loading frequency, the loading and unloading speed gradually increases from $0.4\sigma_c$/s (1Hz) to $8\sigma_c$/s (20Hz), and the opening of the hysteretic ring gradually increases. This indicates that the damage of the sample becomes larger, as shown in Figure 6 (e).

To reflect the above characteristics more clearly, the hysteretic loops of the sample at different frequencies are drawn, as shown in Figure 7 (taking the first cycle as an example). From Figure 7, The higher the loading frequency, the more ‘full and round’ the shape of the hysteretic loop under the same cycle number, the smaller the strain response speed is, and the larger the strain variable of plastic damage is. The evolution law of the hysteretic loop actually reflects a process of gradual adjustment of the initiation and distribution speed and stress of microcracks within the crystal lattice and intergranular of the sample.

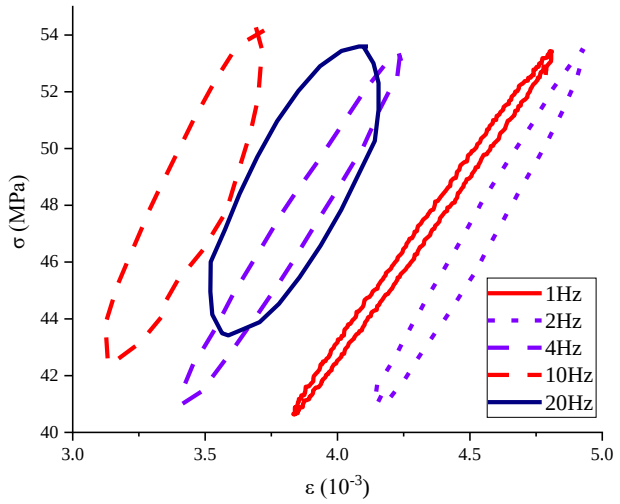


Figure 7. Hysteresis loops at different frequencies

To further explore the influence of loading frequency on strain, the axial strain at the time of failure was extracted, and the strain ε_0 at the beginning of fatigue loading was taken as the reference to calculate the cumulative strain increment L of each typical sample. The calculation formula is as follows:

$$L = \frac{\varepsilon - \varepsilon_0}{\varepsilon_0} \qquad (3)$$

Define the average strain increment $\bar{L}$. $\bar{L}$ represents sample after a single loading cycle average increase of the strain. Easy to know:

$$\bar{L} = \frac{L}{n} \qquad (4)$$

The cumulative strain increment L and average strain increment $\bar{L}$ of the sample were calculated according to Equations (3) and (4), and the results were shown in Table 3.

Table 3. Strain increment result

Group	*f*/Hz	*L*	$\bar{L}(10^{-3})$
1	1	0.084	28.05
2	2	0.143	2.801
3	4	0.197	0.964
4	10	0.202	0.504
5	20	0.206	0.317

The variation curves of cumulative strain increment and average strain increment with frequency were drawn and fitted, as shown in Figure 8.

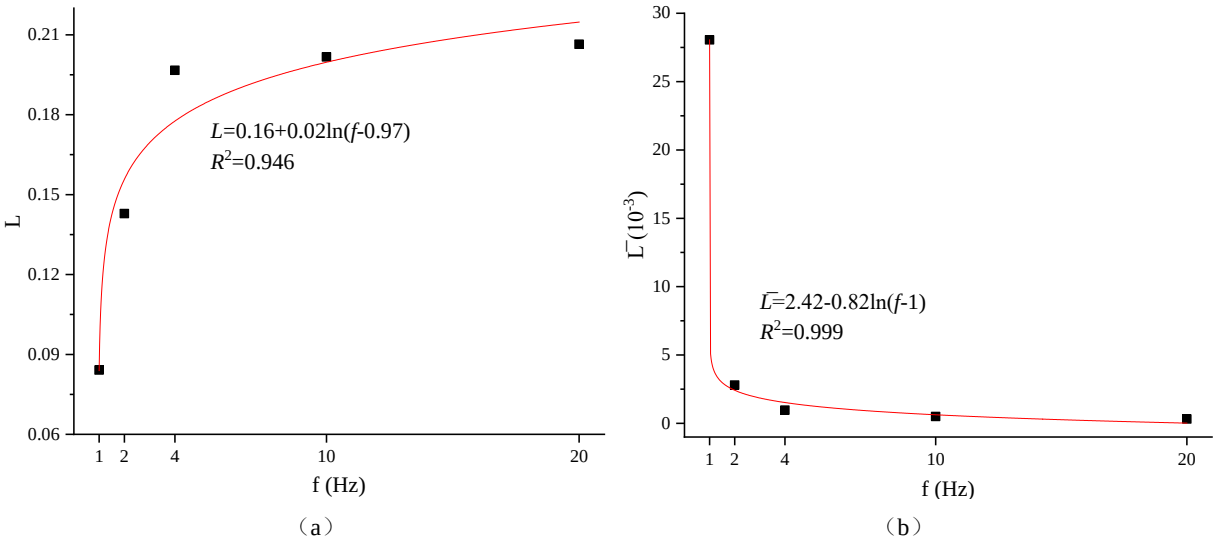


Figure 8. Strain increment. (a)L. (b)$\bar{L}$

As can be seen from Figure 8, cumulative strain increment and average strain increment of the sample show two opposite trends with the increase of frequency. Among them, cumulative strain increment increases with the increase of frequency, but the rate of increase decreases gradually; average strain increment decreases with the increase of frequency, and the rate of decrease also slows down gradually. The logarithmic function is used to fit it, and the relationship is as follows:

$$L=0.16+0.02\ln(f-0.97) \quad (5)$$

$$\bar{L}=2.42-0.82\ln(f-1) \quad (6)$$

The confidence of Equations (5) and (6) both exceed 0.9, indicating that the logarithmic fitting function can better reflect the change rule of the two.

Figure 8 (a) and Figure 8 (b) reflect two seemingly "radically different" results. That is, with the increase of loading frequency, the energy dissipation of specimens in the whole fatigue loading gradually increases (the total hysteretic loop offset increases, that is, the cumulative strain increment increases). However, the energy dissipation between each hysteresis loop decreases gradually (the offset between hysteresis loops decreases, that is, the average strain increment decreases). This phenomenon can also be seen in the thumbnail of Figure 8. The right offset between hysteresis loops is negatively correlated with frequency, which means that with the increase of frequency, the increase rate of average strain of the sample gradually decreases, leading to the fatigue number n that the sample can withstand gradually increases with the increase of frequency. At the same time, the increase of frequency also means that the loading time required for the same cycle becomes shorter, so the fatigue life T shows a downward trend when f exceeds 4Hz.

3.2 Stress-circumferential strain characteristics

In the process of radial fatigue loading, the annular strain is an important index to reflect the yield and failure characteristics of rock samples. To further analyze the relationship between loading frequency f and test fatigue damage, the stress-circumferential strain curve of the sample at typical moments was drawn, as shown in Figure 9. Compared with the stress-axial strain hysteresis curve, the stress-circumferential strain hysteresis curve is relatively zigzagging and not smooth. This is because, compared with the axial deformation, the circumferential deformation of the sample is not directly related to the axial pressure, and the stress-circumferential deformation deviates quicker from the linear elastic state. Comparing the hysteretic curve of the typical sample at different frequencies shows that at a low loading frequency, the inclination angle of the hysteretic curve is tilted to the ε axis, the load of the sample changed slowly and the strain of the sample changed strongly. For example, when f = 1 Hz and f = 2 Hz were used, the differences between the annular strain peak value and the valley value of the average single hysteretic ring were 2.19×10^{-5} and 2.13×10^{-5}, respectively. With the loading frequency increase, the

dip angle of the hysteretic loop gradually inclined toward the σ axis, the loading rate of the sample increased, and the variation range of the sample gradually decreased. For example, when f = 10 Hz and f = 20 Hz were used, the differences between the peak value and valley value of the annular strain of the average single hysteretic loop were 1.18×10^{-5} and 4.61×10^{-6}, respectively. This indicates that the lower the frequency, the greater the damage of the specimen in a single cycle.

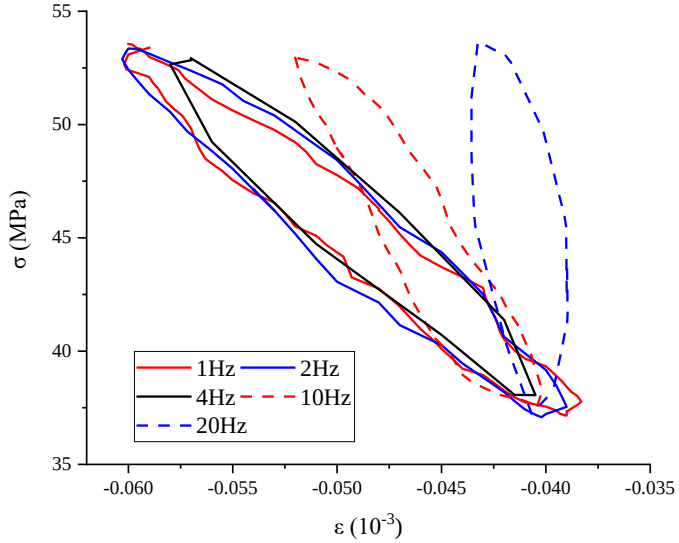


Figure 9. Stress-circumferential deformation curves at typical moments

3.3 Acoustic emission characteristics

Numerous studies have shown that the ringing count and energy of AE parameters are of great significance for the evaluation of fracture and damage degree of materials. Therefore, this study selected the ringing count and energy as the research object to study the AE phenomenon of samples in the fatigue loading process. Combined with *σ-t* curve, the relationship between the acoustic emission phenomenon and the stress on the specimen at the same time is studied, and the damage evolution process of the rock sample is revealed from the macro and micro perspectives. Figure 10 shows the relationship between energy, ringing count, stress and time of gypsum rock under fatigue loading. To save space, this Figure only shows the typical curve of the sample under f = 1Hz and 20Hz.

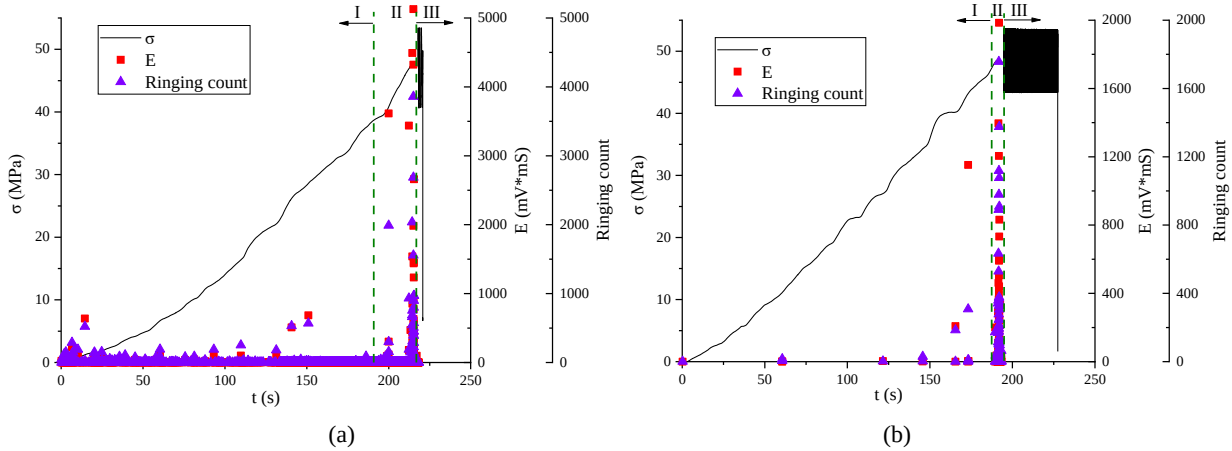


Figure 10. Acoustic emission characteristics of gypsum-like rocks. (a)f=1Hz. (b)f=20Hz.

It can be seen from Figure 10 that the ringing times and energy parameters of gypsum rock are greatly correlated with the loading process, and the specific characteristics are as follows:

(1) In the initial loading stage, I: The ringing count occurred was relatively stable on the whole, and the ringing count of an acoustic emission event was generally less than 200 times, indicating that the rock-like damage was slight at this stage. Acoustic emission events are mainly related to rock - like fractures,

filling, compaction and pore closure. In the process of closure, the destruction of some rough surfaces and the closure of pores will produce a small amount of acoustic emission information, and the energy-time curve response is lower.

(2) Crack growth stage, II: The axial stress of gypsum-like rock is around 47MPa, which is close to the stage of fatigue loading. At this time, the AE activity was significantly enhanced, the ringing count and energy suddenly increased. The slope of the stress-time curve of some samples began to decrease, indicating that the rock samples had caused some local damage when they were loaded to close to $0.8\sigma_c$, but the overall stability was still there.

(3) Fatigue loading stage, III: Acoustic emission activity starts to be stable again, and the change of ringing count and energy is gradually uniform. The reason is that the stress of the sample is the axial stress loaded by the sinusoidal wave with constant amplitude and frequency, the damage of the rock is relatively uniform, and the corresponding acoustic emission parameters are also relatively stable.

Figure 11 shows the strain-strain rate and acoustic emission characteristic curves of a typical test at the beginning of the cycle. Where, the strain rate ε*(t) is the derivative of strain ε with respect to time t, and the calculation formula is as follows:

$$\varepsilon * (t) = \frac{\mathrm{d}\varepsilon}{\mathrm{d}t} \qquad (7)$$

Approximately, Equation (8) can be used to calculate the strain rate corresponding to each strain sampling point.

$$\varepsilon * (t) = \frac{\varepsilon(t+\triangle t)-\varepsilon(t)}{\triangle t} \qquad (8)$$

As can be seen from Figure 11, the peak strain of the sample in each cycle shows an upward trend with the increase of loading time. Taking the sample in Figure 11 (b), i.e., f=2Hz, as an example, the mechanism of the loading of stable frequency and stress amplitude on the sample is analyzed as follows:

(1) Initial stage (t=200~210s): In this stage, the strain growth rate of the sample is fast, but with the increase of the loading time, the growth rate gradually slows down, and the strain rate curve as a whole also shows a downward trend. At this stage, the response of acoustic emission is much lower than that before fatigue, but it still maintains a certain level.

(2) Stable development phase (t=210~225s): At this stage, the peak strain of the sample in each cycle remains roughly stable with the increase of loading time, the upper and lower boundaries of the strain-time curve are approximately linear, and the strain rate curve is also stable. At this stage, the acoustic emission response level further decreases and reaches the lowest level in the whole curve.

(3) the failure stage (t=225~226s): At this stage, the peak strain of the sample increases rapidly with the failure of the sample, and the strain rate curve begins to mutate after a certain period of "load accumulation", increasing by more than 110% within 1~2s. At this stage, the sample ruptures and a large number of micro-ruptures occur, and the acoustic emission characteristics rise again, reaching a higher level.

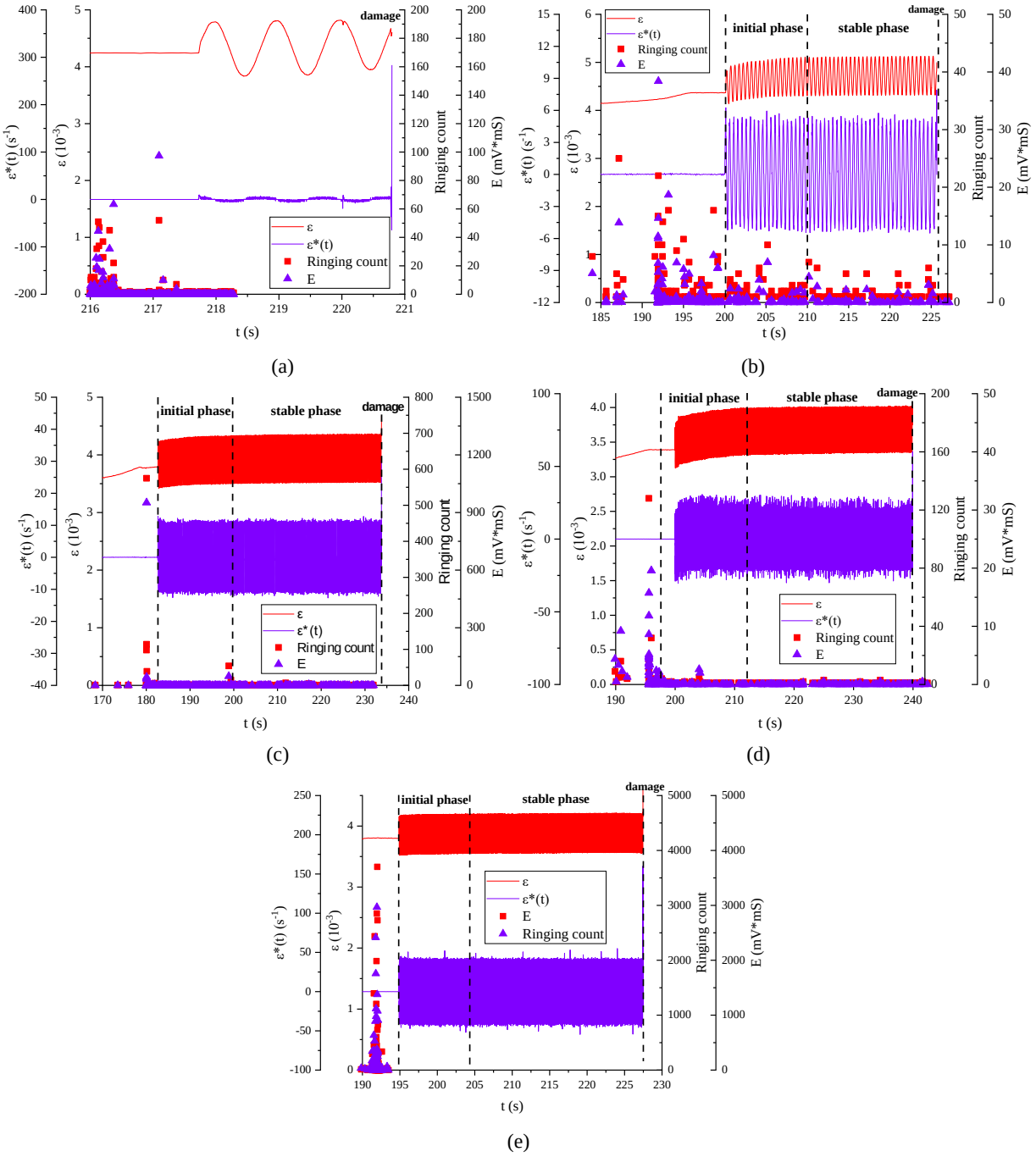


Figure 11. Strain of sample and ae characteristics. (a)*f*=1Hz. (b)*f*=2Hz. (c)*f*=4Hz. (d)*f*=10Hz. (e)*f*=20Hz.

3.4 Failure characteristics

3.4.1 The macro characteristics

Figure 12 shows the failure pictures of typical samples at different frequencies.

As can be seen from Figure 12, the specimens without fatigue loading show shear failure after uniaxial compression, and the shear plane starting from the edge of the specimen end face shows typical diagonal shear failure. The controlled shear fracture surface has a fine powdery substance with obvious friction marks, whereas the tensile fracture surface is fresh. However, after fatigue loading, the end-face effect of the specimens is more obvious, and the failure modes of the specimens are the fatigue damage with near vertical cracks and shear failure with large cracks. This indicates that the accumulated damage of the specimen damaged by fatigue loading is greater than that of the specimen damaged by uniaxial compression.

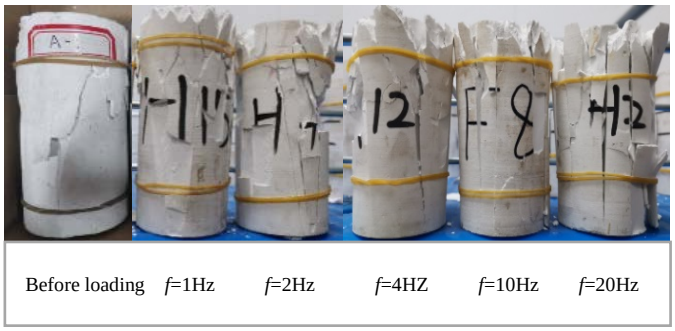


Figure 12. Macroscopic failure characteristics of samples

3.4.2 The microscopic characteristics

The above analysis shows that changing the frequency of cyclic loading has a great effect on the fatigue life of gypsum rock samples. To further explore the influence mechanism of loading frequency on the mechanical properties of gypsum rock, FEI Quanta 250 FEG-SEM scanning electron microscope was used to scan the microstructure of each sample. Figure 13 shows the scanning results before and after fatigue at a magnification of 6000 times.

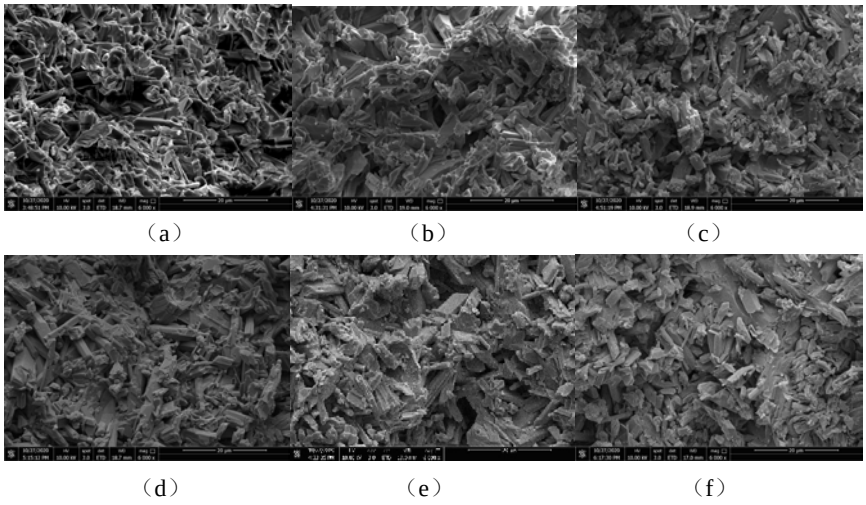


Figure 13. Scanning electron microscope images of samples before and after fatigue. (a)Before loading. (b)*f*=1Hz. (c)*f*=2Hz. (d)*f*=4Hz. (e)*f*=10Hz. (f)*f*=20Hz.

As can be seen from Figure 13, there are a lot of flocculation structures on the surface of the specimens damaged by common uniaxial compression. The surface structure of the sample is relatively compact as a whole, only some particles are loose. Most particles have rounded edges without sharp edges, as shown in Figure 13 (a). After fatigue loading, the surface of the specimen changes obviously. As shown in Figure 13 (b), after 1Hz fatigue loading, obvious columnar crystals appeared on the surface of the sample, and the crystal structure tended to be loose and disordered, with crystal edges and angles gradually distinct. With the increase of fatigue loading frequency, the number of fatigue loading times that the sample can bear increases gradually, and the distribution of columnar and intergranular microcracks on the sample surface also increases gradually. Especially when f =10Hz, a large number of crystal cracks appear on the surface of the sample, the number of micropores increases significantly, and secondary cracks gradually appear and develop. When f =20Hz, under the action of more than 600 cyclic stress, some secondary fractures develop and are gradually compacted, and even form partial massive structures.

The above phenomena indicate that the specimens exhibit obvious fatigue damage under the fatigue load of 0.7~0.9 σ_c. As the fatigue loading frequency increases, the loading and unloading speed increases from 0.4 σ_c/s (1 Hz) to 8 σ_c/s (20 Hz). With the increase of loading rate, the damage of the sample in a single hysteretic loop decreases gradually, and the number of fatigue loading times it can bear increases gradually. As a result, the crystal structure and shape of the sample gradually changed, and the number of microcracks and micropores in the sample gradually

increased. Microscopically, the flocculent structure gradually disappeared and the disorderly columnar structure appeared in large numbers. With the increase of cyclic loading times, the original cracks in the sample gradually expand and penetrate, and the secondary cracks also gradually develop, resulting in the width, length and coverage of the sample cracks gradually increase, and the macroscopic damage continues to develop, leading to the deterioration of physical and mechanical properties.

4.Discussion

As shown in Figure 6, with increasing fatigue frequency, the area surrounded by the hysteresis loop gradually increases, indicating that amount of damage of the sample increase in a single hysteresis loop. To quantitative analyze on this change, the approximate area of each hysteretic loop is calculated by calculus.

As shown in Figure 14(a), the upper curve of the hysteresis loop is denoted by A(ε) and the lower curve is denoted by B(ε). Then, the calculation formula for the hysteresis loop area is:

$$S = \int_a^b A(\varepsilon)\, d\varepsilon - \int_a^b B(\varepsilon)\, d\varepsilon \qquad (9)$$

It can be approximated that:

$$S = \sum_{n=a}^{b} \triangle \varepsilon \left(\frac{A(n+\triangle\varepsilon)+A(n)}{2} - \frac{B(n+\triangle\varepsilon)+B(n)}{2} \right) \qquad (10)$$

In Equation (10), $\triangle\varepsilon$ is the change in strain. Since the sampling rate of the experimental system used in the manuscript is 10Hz, $\triangle\varepsilon$ refers to the change value of strain after 0.1s. According to Formula (10), the hysteresis loop area of each sample during the first cycle is calculated, and the results are shown in Figure 14(b).

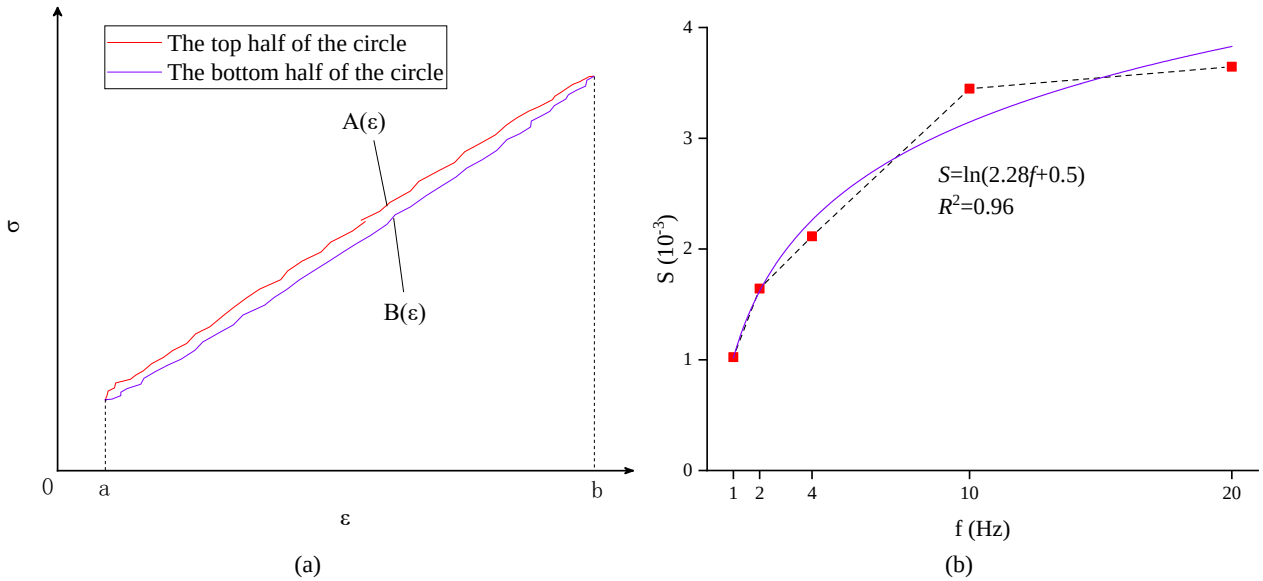


Figure 14. Hysteresis loop area.(a) Calculation schematic diagram.(b) Result diagram.

Figure 14(b) shows that the hysteresis loop area *S* is positively correlated with frequency *f* in vibration. At *f*=1Hz, the average hysteresis loop area was 1.02, which was 256%, 237%,107% and 60.5% larger compared with *f* =2, 4, 10 and 20 Hz, respectively. The growth rate of S reaches the maximum in the interval of $f \in [1,4]$ and decreases gradually when f exceeds 4 Hz.

The logarithmic fitting of area *S* and frequency *f* is as follows:

$$S=\ln(2.28f+0.5) \qquad (11)$$

The confidence of Equations (11) exceeds 0.95, indicating that the logarithmic fitting function can better reflect the change rule of the two.

The anti-fatigue coefficient *D* is defined to characterize the ability of the specimen to resist fatigue failure. The calculation formula is as follows:

$$D_m = n_m(S+\bar{L}) = n_m S + L \qquad (12)$$

where, $m=\{1,2,4,10,20\}$, $(n_1, n_2, n_4, n_{10}, n_{20})^T = (T_1, T_2, T_4, T_{10}, T_{20})^T$ (1, 2, 4, 10, 20).

The anti-fatigue coefficient D of the samples under each loading frequency is calculated by formula (12) as follows:

$$(D_1, D_2, D_4, D_{10}, D_{20})^T = (0.087, 0.227, 0.628, 1.57, 2.58)^T \qquad (13)$$

It can be seen from formula (13) that with the increase of frequency f, the ability of the specimen to resist fatigue failure increases gradually. At high frequencies, a single hysteresis loop has a large area and consumes more energy, but the hysteresis loop shows less right deviation; therefore, the damage per unit time is less. At low frequencies, although the area of a single hysteretic ring is small, the space between each hysteretic ring is large, and the overall energy consumption increases. This leads to the increase of the ultimate fatigue number of the specimen with the increase of frequency.

Formula (13) is the calculation result of anti-fatigue coefficient based on ultimate fatigue times. The formula for calculating the anti-fatigue coefficient based on fatigue life T is as follows:

$$D'_m = \frac{D_m}{f_m} \qquad (14)$$

Formula (14) is used to calculate D'_m, and the result is as follows:

$$(D'_1, D'_2, D'_4, D'_{10}, D'_{20})^T = (0.087, 0.113, 0.157, 0.157, 0.129)^T \qquad (15)$$

It can be seen from formula (15) that with the increase of frequency f, the anti-fatigue coefficient D' based on fatigue life is prolonged at first and then shortened, and reaches the peak value at f=4Hz, which is in close agreement with the above analysis results. Although the ultimate fatigue times of the sample are positively correlated with the frequency, the fatigue times per unit time gradually increase with the increase of frequency, which leads to a downward trend of fatigue life of the sample when f > 4Hz.

5.Conclusion

For this article, the samples were remolded by casting A-class α high strength gypsum powder, and fatigue loading and acoustic emission tests were carried out by using the rock dynamic fatigue testing machine to explore the influence of loading frequency on the fatigue life of rock. The conclusions are as follows:

(1) Under cyclic loading, the cumulative strain increment is positively correlated with loading frequency, while the average strain increment is negatively correlated with loading frequency. This results in a positive correlation between the maximum fatigue loading times and the loading frequency, while the fatigue life reaches the maximum at f=4Hz, increases in $f \in [1,4]$, and decreases in $f \in [4,20]$.

(2) The stress-circumferential strain hysteresis loop of the specimen tilts to ε axis at low frequency and to σ axis at high frequency, indicating that the lower the frequency, the greater the damage of the specimen in one cycle.

(3) The peak strain of the sample in each cycle increases with the increase of loading time. Under given fatigue loading frequency and amplitude, the deformation and failure characteristics of the specimen can be divided into three stages: initial stage, stable development stage and failure stage. The acoustic emission characteristics are in good agreement with the above stages in the σ-t curve.

(4) Under the condition of conventional uniaxial compression test, gypsum - like rocks mostly show shear failure. However, the end-face effect of uniaxial compression specimens under fatigue loading is more obvious, and the failure modes are mainly the fatigue damage of near vertical cracks. After fatigue loading, the specimen has obvious fatigue damage. With the expansion and penetration of the internal crack, the width, length and coverage of the crack gradually increase, leading to the continuous deterioration of the physical and mechanical properties.

References

Bagde M N, Petros V (2005) Waveform effect on fatigue properties of intact sandstone in uniaxial cyclical loading. Rock Mechanics and Rock Engineering. 38(3):169–196.

Bai Yueming (2012) Experimental research on the fatigue property of salt rock under cyclic loading [M. S. Thesis] [D]. Chongqing：Chongqing Universit.

Guo Yintong, ZHAO Kelie, SUN Guanhua (2011) Experimental study of fatigue deformation and damage characteristics of salt rock under cyclic loading[J]. Rock and Soil Mechanics. 32(5): 1 353–1 359.

Ishizuka Y, ABE T (1990) Fatigue behaviour of granite under cyclic loading[C]// Static and Dynamic Considerations in Rock Engineering. Rotterdam：A. A. Balkema:139–147.

Jiang Yu (2003) Fatigue failure and deformation development law of rock under cyclic load [M. S. Thesis] [D]. Shanghai：Shanghai Jiaotong University.

LI Haoran, Yang Chunhe, LI Bailin (2016) Damage evolution and characteristics of ultrasonic velocity and acoustic emission for salt rock under triaxial multilevel loading test[J]. Chinese Journal of Rock Mechanics and Engineering. 35(4)：683–691.

Li Tiantao, Pei Xiangjun, Guo Jian (2020) An Energy-Based Fatigue Damage Model for Sandstone Subjected to Cyclic Loading. 53(prepublish):1-11.

Li N, Chen W, Zhang P (2001) The mechanical properties and a fatigue-damage model for jointed rock masses subjected to dynamic cyclical loading[J]. International Journal of Rock Mechanics and Mining Sciences.38(7)：1071–1 079.

Liu Yi, Dai Feng, Fan Pengxian, Xu Nuwen, Dong Lu (2017) Experimental Investigation of the Influence of Joint Geometric Configurations on the Mechanical Properties of Intermittent Jointed Rock Models Under Cyclic Uniaxial Compression[J]. Rock Mechanics and Rock Engineering.50(6).

Liu Yi, Dai Feng (2018a) A damage constitutive model for intermittent jointed rocks under cyclic uniaxial compression[J]. International Journal of Rock Mechanics and Mining Sciences.103:

Liu Yi, Dai Feng, Lu Dong (2018b) Experimental Investigation on the Fatigue Mechanical Properties of Intermittently Jointed Rock Models Under Cyclic Uniaxial Compression with Different Loading Parameters[J]. Rock Mechanics and Rock Engineering. 51(1) : 47-68.

Liu Yi, Dai Feng (2021) A review of experimental and theoretical research on the deformation and failure behavior of rocks subjected to cyclic loading[J]. Journal of Rock Mechanics and Geotechnical Engineering. 13(5) : 1203-1230.

Liu Yunping, XI Daoying, ZHANG Chengyuan (2001) Dynamic response of marble sandstone under cyclic stress [J]. Journal of Rock Mechanics and Engineering.(02):216-219.

Ma W. B., Chai J. F., Han Z. L. (2020) Research on Design Parameters and Fatigue Life of Tunnel Bottom Structure of Single-Track Ballasted Heavy-Haul Railway Tunnel with 40-Ton Axle Load. 2020.

Roohollah Shirani Faradonbeh, Abbas Taheri, Murat Karakus (2020) Post-peak behaviour of rocks under cyclic loading using a double-criteria damage-controlled test method:1-15.

Wei Sijiang, Wang Chongyang, Yang Yushun (2020) Physical and Mechanical Properties of Gypsum-Like Rock Materials [J]. Advances in civil engineering. 2020.

Xi Daoying, Liu Xiaoyan, Zhang Chengyuan (2003) Analysis on micro and meso-damage of rock by Macro-hysteresis curve. Journal of Rock Mechanics and Engineering: (02):182-187.

Xiao Jianqing (2009) Theoretical and experimental study of rock fatigue characteristics under cyclic loading [Ph. D. Thesis] [D]. Changsha：Central South University.

Xu Jiang, Xian Xuefu, Wang Hong, Wang Weizhong (2006) Experimental study on rock deformation characteristics under cycling loading and unloading conditions. Journal of Rock Mechanics and Engineering. (S1):3040-3045.

Yang Yongjie, SONG Yang, CHU Jun (2007) Experimental study on characteristics of strength and deformation of

coal under cyclic loading[J]. Journal of Rock Mechanics and Engineering. (01):201-205.
Zhang Qi, Dai Feng, Liu Yi (2022) Experimental assessment on the dynamic mechanical response of rocks under cyclic coupled compression-shear loading[J]. International Journal of Mechanical Sciences.216.
Zhao Chuang, WU Ke, LI Shucai (2013) Analysis of rock damage deformation and energy characteristics under cyclic loading [J]. Journal of geotechnical engineering.35(05):890-896.
Zhao Kai (2013) Experimental study on fatigue characteristics of karst areas limestone and engineering application [Ph. D. Thesis] [D]. Beijing：Beijing Jiaotong University.
Zuo Jianping, PEI Jianliang, LIU Jianfeng (2011) Investigation on acoustic emission behavior and its time-space evolution mechanism in failure process of coal-rock combined body[J]. Chinese Journal of Rock Mechanics and Engineering.30(8): 1564–1570.